 CMES, vol.14, no.3, pp.161-169, 2006

On the NGF Procedure for LBIE Elastostatic Fracture Mechanics

L.S. Miers[1] **and J.C.F. Telles**[2]

Abstract: This work aims at extending the concept of the Numerical Green's Function (NGF), well known from boundary element applications to fracture mechanics, to the Local Boundary Integral Equation (LBIE) context. As a "companion" solution, the NGF is used to remove the integrals over the crack boundary and is introduced only for source points whose support touches or contains the crack. The results obtained with the coupling of NGF-LBIE in previous potential discontinuity Laplace's equation problems and the authors' experience in NGF-BEM fracture mechanics were the motivation for this development.

keyword: LBIE, Meshless methods, Numerical Green's function, Fracture mechanics.

1 Introduction

Meshless methods are increasingly proving to be quite accurate in the analysis of the most common problems found in engineering applications. They can be very efficient, in terms of computer time, in solving problems that need a great number of node repositioning during the analysis, which can be more expensive than the analysis itself when using mesh-based methods.

Normally, a meshless method is a mesh-free counterpart of a well-established mesh-based method [Atluri and Shen (2002); Atluri, Sladek, Sladek and Zhu (2000)] and because of this, there is no reason to believe that the improvements made for the mesh-based procedures cannot be implemented in their mesh-free versions.

In this work, the concept of the numerical Green's function (NGF) for 2-D elastostatic fracture mechanics is introduced in the local boundary integral equation (LBIE) method, which has been brought into existence from the boundary integral equation, basic to the boundary element method (BEM). Many meshless fracture mechanics applications can be recently found in the literature [Gao, Liu and Liu (2006); Andreaus, Batra and Porfiri (2005); Sladek, Sladek, Krivacek and Zhang (2005)]. The NGF for fracture mechanics was first used in a BEM approach [Telles, Castor and Guimarães (1995)] during the last decade and has recently been used for potential discontinuity simulations, already applied to the LBIE, generating very good results [Miers and Telles (2005)].

The approximation scheme for the trial function used here is the well-known moving least squares (MLS) method, which is the most common alternative in the bibliography [Lancaster and Salkauskas (1981)]. The singular integrals are computed using Kutt's quadrature [Brebbia, Telles and Wrobel (1984)] procedure, well-known from previous BEM implementations.

2 LBIE for liner elasticity problems

Consider the following 2-D linear elasticity problem defined within the domain Ω and boundary Γ,

$$\sigma_{ij,j} + b_j = 0 \tag{1}$$

where σ_{ij} is the stress tensor, b_i is the body force and $()_{,i}$ denotes the derivative with respect to x_i. The boundary conditions are

$$\begin{aligned} &u_i = \overline{u}_i \text{ on } \Gamma_u \\ &p_i \equiv \sigma_{ij} n_j = \overline{p}_i \text{ on } \Gamma_p \end{aligned} \tag{2}$$

where the bar indicates prescribed values, respectively, for displacements u and tractions p and Γ_u and Γ_p are the parts of the boundary Γ where they are prescribed.

Using u_i^G as test function, the weak form of Equation (1) can be written as

$$\int_\Omega (\sigma_{ij,j} + b_j)\ u_i^G d\Omega = 0 \tag{3}$$

and integrating Eq.(3) by parts twice, the following expression is obtained:

$$-\int_\Omega \sigma_{ij,j}^G u_i d\Omega + \int_\Gamma p_i^G u_i d\Gamma = \int_\Gamma p_i u_i^G d\Gamma + \int_\Omega b_i u_i^G d\Omega \tag{4}$$

[1] COPPE/UFRJ, email: lsmiers@coc.ufrj.br
[2] COPPE/UFRJ, email: telles@coc.ufrj.br

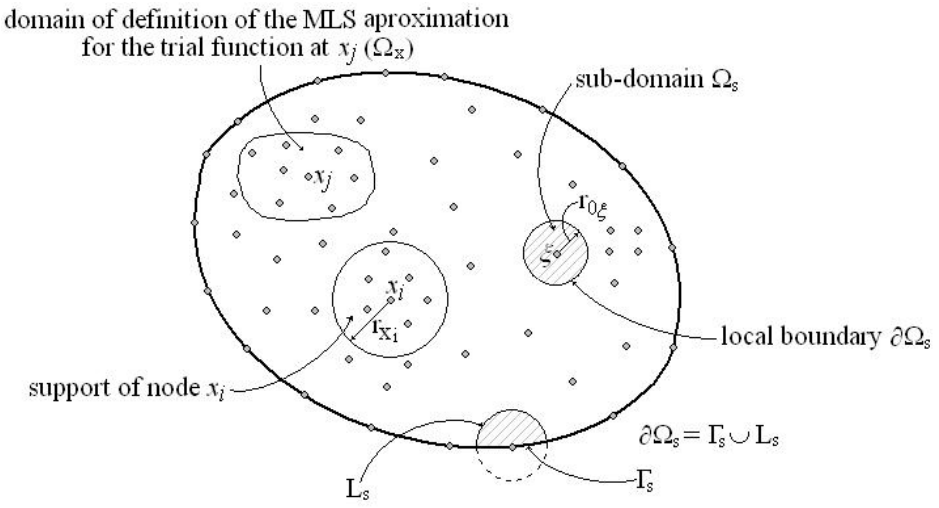

Figure 1 : Sub-domains, boundaries, supports and the domains of definition of the MLS approximation

In the present case, u_i^G is chosen to be the solution of a unit load in an infinite plane containing cracks, to be discussed later on. This solution satisfies the following condition

$$\sigma_{ij,j}^G(\xi,\mathbf{x}) + \delta(\xi,\mathbf{x})e_i = 0 \tag{5}$$

where $\delta(\xi,\mathbf{x})$ is the Dirac delta function and e_i is the unit load vector on the x_i direction. The test functions can be rewritten as

$$\begin{aligned} u_i^G &= u_{ki}^G e_k \\ p_i^G &= p_{ki}^G e_k \end{aligned} \tag{6}$$

where u_{ki}^G and p_{ki}^G are, respectively, the i-th components of displacements and tractions due to a unit load in the x_k direction.

Substituting Eqs.(6) and (5) in Eq.(3) leads to the so-called Somigliana's identity, which gives the values of displacements in any point of the domain in terms of the boundary values of displacements and tractions:

$$\begin{aligned} u_i(\xi) = &\int_\Gamma u_{ij}^G(\xi,\mathbf{x}) p_j(\mathbf{x}) d\Gamma - \int_\Gamma p_{ij}^G(\xi,\mathbf{x}) u_j(\mathbf{x}) d\Gamma \\ &+ \int_\Omega u_{ij}^G(\xi,\mathbf{x}) b_j(\mathbf{x}) d\Omega \end{aligned} \tag{7}$$

where ξ is the source point and $\mathbf{x}$ is the field (generic) point.

If instead of the real domain Ω and boundary Γ of the problem, a sub-domain Ω_s and its boundary $\partial\Omega_s$ located entirely inside Ω (see Fig.1) are considered, Eq.(7) becomes

$$\begin{aligned} u_i(\xi) = &\int_{\partial\Omega_s} u_{ij}^G(\xi,\mathbf{x}) p_j(\mathbf{x}) d\Gamma - \int_{\partial\Omega_s} p_{ij}^G(\xi,\mathbf{x}) u_j(\mathbf{x}) d\Gamma \\ &+ \int_{\Omega_s} u_{ij}^G(\xi,\mathbf{x}) b_j(\mathbf{x}) d\Omega \end{aligned} \tag{8}$$

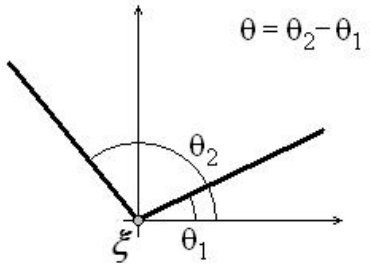

Figure 2 : Definition of e θ, θ_1 and θ_2.

For a source point located on the global boundary Γ, Eq.(8) can be rewritten as

$$\begin{aligned} \alpha_{ij}(\xi) u_i(\xi) = &\int_{L_s+\Gamma_s} u_{ij}^G(\xi,\mathbf{x}) p_j(\mathbf{x}) d\Gamma \\ &- \int_{L_s+\Gamma_s} p_{ij}^G(\xi,\mathbf{x}) u_j(\mathbf{x}) d\Gamma + \int_{\Omega_s} u_{ij}^G(\xi,\mathbf{x}) b_j(\mathbf{x}) d\Omega \end{aligned} \tag{9}$$

and considering two dimensions only, its matrix form is as follows,

$$\alpha\mathbf{u} = \int_{L_s+\Gamma_s} \mathbf{u^G p} d\Gamma - \int_{L_s+\Gamma_s} \mathbf{p^G u} d\Gamma + \int_{\Omega_s} \mathbf{u^G b} d\Omega \tag{10}$$

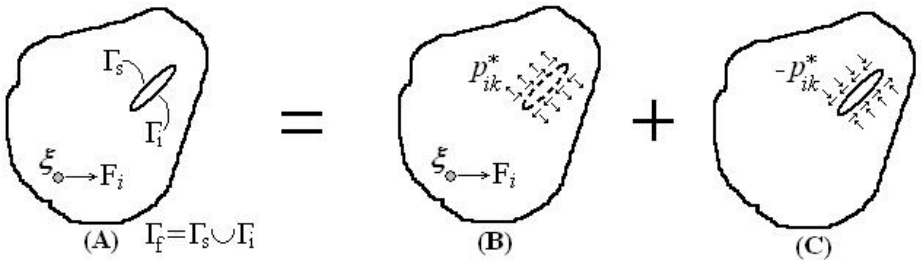

Figure 3 : Superposition of effects

where

$$\mathbf{u}^G = \begin{bmatrix} u^G_{11} & u^G_{12} \\ u^G_{21} & u^G_{22} \end{bmatrix}; \quad \mathbf{p}^G = \begin{bmatrix} p^G_{11} & p^G_{12} \\ p^G_{21} & p^G_{22} \end{bmatrix};$$
$$\mathbf{u} = \begin{bmatrix} u_1 \\ u_2 \end{bmatrix}; \quad \mathbf{p} = \begin{bmatrix} p_1 \\ p_2 \end{bmatrix}; \quad \mathbf{b} = \begin{bmatrix} b_1 \\ b_2 \end{bmatrix}. \tag{11}$$

and α_{ij} (α) is a constant matrix that depends on the shape of the boundary at ξ.

$$\alpha(\xi) = \begin{bmatrix} \frac{\theta}{2\pi} - \frac{\sin 2\theta_1 - \sin 2\theta_2}{8\pi(1-\overline{\nu})} & \frac{\cos 2\theta_1 - \cos 2\theta_2}{8\pi(1-\overline{\nu})} \\ \frac{\cos 2\theta_1 - \cos 2\theta_2}{8\pi(1-\overline{\nu})} & \frac{\theta}{2\pi} + \frac{\sin 2\theta_1 - \sin 2\theta_2}{8\pi(1-\overline{\nu})} \end{bmatrix} \tag{12}$$

where θ, θ_1 and θ_2 are defined in Fig.2 and

$$\overline{\nu} = \begin{cases} \nu & \text{for plane strain} \\ \frac{\nu}{1+\nu} & \text{for plane stress} \end{cases} \tag{13}$$

In most situations found in current elastostatics literature [Atluri, Sladek, Sladek and Zhu (2000), Vavourakis, Sellountos and Polyzos (2006)], the functions $(\ )^G$ adopted are Kelvin's fundamental solution for an infinite plane plus a "companion" solution, whose sole purpose is to vanish the fundamental displacements at L_s in order to eliminate the integration of the traction terms over L_s. This approach is not used here due to the built-in presence of the crack, which mathematically leads to another term to be added to the Kelvin fundamental solution.

3 Numerical Green's function for fracture mechanics

Consider an infinite elastic plane with an unloaded crack inside under the action of a unit point load applied at ξ. The fundamental displacements and tractions for this case can be calculated by the superposition shown in Fig.3, which mathematically reads

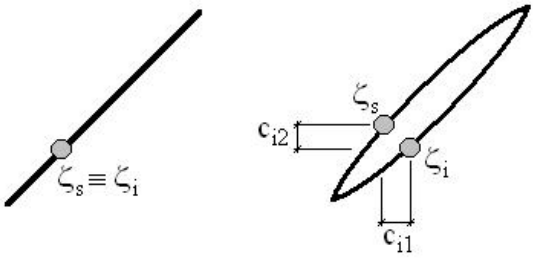

Figure 4 : Crack openings

$$u^G_{ij}(\xi,\mathbf{x}) = u^*_{ij}(\xi,\mathbf{x}) + u^c_{ij}(\xi,\mathbf{x})$$
$$p^G_{ij}(\xi,\mathbf{x}) = p^*_{ij}(\xi,\mathbf{x}) + p^c_{ij}(\xi,\mathbf{x}) \tag{14}$$

where $(\ )^*$ refers to Kelvin's fundamental solution (Fig.3B) and $(\ )^c$ indicates the complementary part (Fig.3C).

According to [Telles, Castor and Guimarães (1995)], the complementary part of the solution can be calculated as follows

$$u^c_{ij}(\xi,\mathbf{x}) = \int_{\Gamma_i} p^*_{jk}(\mathbf{x},\zeta)\cdot c_{ik}(\xi,\zeta)d\Gamma(\zeta)$$
$$p^c_{ij}(\xi,\mathbf{x}) = \int_{\Gamma_i} P^*_{jk}(\mathbf{x},\zeta)\cdot c_{ik}(\xi,\zeta)d\Gamma(\zeta) \tag{15}$$

where ζ is a point on Γ_i and $c_{ik}(\xi,\zeta)$ are the crack openings (see Fig.4)

$$c_{ik}(\xi,\zeta) = u^c_{ik}(\xi,\zeta^s) - u^c_{ik}(\xi,\zeta^i) \tag{16}$$

which can be calculated by solving the following system of equations

$$\mathbf{Sc}_{ij}(\xi,\zeta) = \mathbf{p}^*_{ij}(\xi,\zeta) \tag{17}$$

Matrix $\mathbf{S}$ is square of dimension $2N$ (N is the number of points on Γ_i) that depends only of the crack's geometry. This complete formulation can be seen in [Telles, Castor and Guimarães (1995)].

Notice that the complementary part vanishes if no part of the crack lies inside the integration boundary $\partial\Omega_s$. Hence, only the nodes whose sub-domains contain part or the whole crack have non-zero complementary parts. For all other nodes the NGF degenerates to the simpler Kelvin solution. Consequently, the burden of computing the complementary part is avoided.

4 Moving least squares (MLS) approximation scheme

The MLS scheme is by far the most used in meshless methods to approximate the trial function $u^h(\mathbf{x})$. Its definition will be briefly presented in this section and, for more details, see [Lancaster and Salkauskas (1981), Atluri and Shen (2002); Atluri, Sladek, Sladek and Zhu (2000); Chen, Eskandarian and Oskard (2004)]. It has the following form

$$u^h(\mathbf{x}) = \sum_{i=1}^{n} \phi_i(\mathbf{x})\hat{u}_i = \mathbf{\Phi}^T \cdot \hat{\mathbf{u}} \quad \forall \mathbf{x} \in \Omega_x;$$
$$\mathbf{x}_i = [x_i, y_i, z_i]^T \tag{18}$$

where Φ is the MLS shape function, $\hat{\mathbf{u}}$ is the "fictitious" nodal values of the trial function and n is the number of nodes inside the domain of definition Ω_x of the considered node. The domain of definition of a certain node $\mathbf{x}$ is composed by the nodes who have $\mathbf{x}$ inside their support.The shape function is defined as

$$\mathbf{\Phi}^T(\mathbf{x}) = \mathbf{p}^T(\mathbf{x})\mathbf{A}^{-1}(\mathbf{x})\mathbf{B}(\mathbf{x}) \text{ or}$$
$$\phi_i(\mathbf{x}) = \sum_{j=1}^{m} p_j \left(\mathbf{A}^{-1}(\mathbf{x})\mathbf{B}(\mathbf{x})\right)_{ji} \tag{19}$$

where m is the size of the complete monomial basis $\mathbf{p}$, e.g.:

$$\mathbf{p}^T = \begin{cases} \begin{bmatrix} 1 & x & y \end{bmatrix}, \text{linear basis: } m = 3 \\ \begin{bmatrix} 1 & x & y & xy & x^2 & y^2 \end{bmatrix}, \\ \qquad\qquad \text{quadratic basis: } m = 6 \end{cases} \tag{20}$$

and

$$\mathbf{A}(\mathbf{x}) = \mathbf{P}^T\mathbf{W}(\mathbf{x})\mathbf{P}$$
$$\mathbf{B}(\mathbf{x}) = \mathbf{P}^T\mathbf{W}(\mathbf{x}) \tag{21}$$

where

$$\mathbf{W}(\mathbf{x}) = \begin{bmatrix} w_1(\mathbf{x}) & 0 & \dots & 0 \\ 0 & w_2(\mathbf{x}) & & \\ \vdots & & \ddots & \\ 0 & & & w_n(\mathbf{x}) \end{bmatrix};$$
$$\mathbf{P} = \begin{bmatrix} \mathbf{p}^T(x_1) \\ \mathbf{p}^T(x_2) \\ \vdots \\ \mathbf{p}^T(x_n) \end{bmatrix} \tag{22}$$

$w_i(\mathbf{x})$ being the weight function associated with node i. In this work a Gaussian function of the following form is used

$$w_i(\mathbf{x}) = \frac{e^{-\left(\frac{d_i}{c_i}\right)^{2k}} - e^{-\left(\frac{r_i}{c_i}\right)^{2k}}}{1 - e^{-\left(\frac{r_i}{c_i}\right)^{2k}}} \text{ for } 0 \le d_i \le r_i$$
$$w_i(\mathbf{x}) = 0 \text{ for } d_i \ge r_i \tag{23}$$

where $d_i = ||\mathbf{x} - \mathbf{x}_i||$, c_i is a constant that controls the shape of w_i, r_i is the size of the support of w_i associated with $\mathbf{x}_i$ and k is a parameter here chosen as 1. There are many other functions suitable for use in MLS approximation, like cubic and quadric spline functions [Atluri and Shen (2002); Atluri, Sladek, Sladek and Zhu (2000); Chen, Eskandarian and Oskard (2004)], but for many applications found in the literature, the best results were obtained with the Gaussian function. The radius of the supports is defined in order to guarantee that all nodes contain at least m nodes in their domains of definition, keeping the discrete approach of the interpolation scheme [Atluri and Zhu (1998)].

The derivative of ϕ_i with respect to x_k is

$$\phi_{i,k} = \sum_{j=1}^{m} \left\{ p_{j,k} \left(\mathbf{A}^{-1}\mathbf{B}\right)_{ji} + p_j \left[\mathbf{A}^{-1}\mathbf{B}_{,k} + \left(\mathbf{A}^{-1}\right)_{,k}\mathbf{B}\right]_{ji} \right\} \tag{24}$$

where

$$\left(\mathbf{A}^{-1}\right)_{,k} = -\mathbf{A}^{-1}\mathbf{A}_{,k}\mathbf{A}^{-1} \tag{25}$$

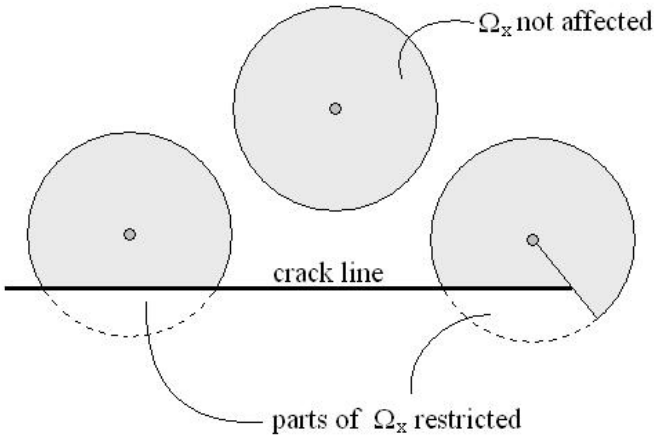

Figure 5 : "Visibility" criterion adopted in presence of the crack

Once having a crack inside Ω, there is a discontinuity of displacements between the regions divided by the crack. Hence, the interpolation scheme must take this issue into consideration. The way this is done in MLS is restricting the support of the nodes by using a so-called "visibility" criterion, as presented in Fig.5.

In this criterion, the crack is considered opaque to an observer that lies on the considered node and only the nodes inside its Ω_x that can be seen are considered in the approximation.

5 Numerical implementation

Consider the parts of the global boundary Γ where the prescribed values are displacements as Γ_u and the traction counterparts as Γ_p. The intersections of these parts with the local sub-domains Ω_s, for each source point (redefined as $\mathbf{x}_i$), are designated respectively as Γ_{su} and Γ_{sp}. Eq.(10) can then be rearranged, leading to the following system of equations

$$\begin{aligned}\alpha_i \mathbf{u}_i = &\int_{L_s} \mathbf{u}^{\mathbf{G}}(\mathbf{x}_i,\mathbf{x})\mathbf{p}(\mathbf{x})d\Gamma - \int_{L_s} \mathbf{p}^{\mathbf{G}}(\mathbf{x}_i,\mathbf{x})\mathbf{u}(\mathbf{x})d\Gamma \\ &+ \int_{\Gamma_{su}} \mathbf{u}^{\mathbf{G}}(\mathbf{x}_i,\mathbf{x})\mathbf{p}(\mathbf{x})d\Gamma - \int_{\Gamma_{sp}} \mathbf{p}^{\mathbf{G}}(\mathbf{x}_i,\mathbf{x})\mathbf{u}(\mathbf{x})d\Gamma \\ &+ \int_{\Gamma_{sp}} \mathbf{u}^{\mathbf{G}}(\mathbf{x}_i,\mathbf{x})\overline{\mathbf{p}}(\mathbf{x})d\Gamma - \int_{\Gamma_{su}} \mathbf{p}^{\mathbf{G}}(\mathbf{x}_i,\mathbf{x})\overline{\mathbf{u}}(\mathbf{x})d\Gamma \\ &+ \int_{\Omega_s} \mathbf{u}^{\mathbf{G}}(\mathbf{x}_i,\mathbf{x})\mathbf{b}(\mathbf{x})d\Omega \end{aligned} \tag{26}$$

where $\overline{\mathbf{u}}(\mathbf{x})$ and $\overline{\mathbf{p}}(\mathbf{x})$ are the prescribed displacements and tractions. Substituting the trial function and its derivatives by their MLS approximations, isolating the unknown terms on the left-hand side, simplifying the notation and rearranging leads to the following system of equations

$$\mathbf{K}\hat{\mathbf{u}} = \mathbf{f} \longleftrightarrow \sum_{j=1}^{N} \mathbf{K}_{ij}\hat{\mathbf{u}}_j = \mathbf{f}_i (i = 1,2,\ldots,N) \tag{27}$$

where

$$\mathbf{f}_i = \begin{cases} \int_{\Gamma_{sp}} \mathbf{u}^G \overline{\mathbf{p}} d\Gamma - \int_{\Gamma_{su}} \mathbf{p}^G \overline{\mathbf{u}} d\Gamma - \int_{\Omega_s} \mathbf{u}^G \mathbf{p} d\Omega - \alpha_i \overline{\mathbf{u}}_i \\ \qquad\qquad \text{where } \mathbf{u}_i \text{ is known} \\ \int_{\Gamma_{sp}} \mathbf{u}^G \overline{\mathbf{p}} d\Gamma - \int_{\Gamma_{su}} \mathbf{p}^G \overline{\mathbf{u}} d\Gamma - \int_{\Omega_s} \mathbf{u}^G \mathbf{p} d\Omega \\ \qquad\qquad \text{where } \mathbf{u}_i \text{ is unknown} \end{cases} \tag{28}$$

and

$$\mathbf{K}_{ij} = \begin{cases} \int_{\Gamma_{sq}} \mathbf{p}^G \phi_j d\Gamma - \int_{\Gamma_{su}} \mathbf{u}^G \mathbf{NDB}_j d\Gamma - \int_{L_s} \mathbf{u}^G \mathbf{NDB}_j d\Gamma \\ \qquad + \int_{L_s} \mathbf{p}^G \phi_j d\Gamma \text{ where } \mathbf{u}_i \text{ is known} \\ \int_{\Gamma_{sq}} \mathbf{p}^G \phi_j d\Gamma - \int_{\Gamma_{su}} \mathbf{u}^G \mathbf{NDB}_j d\Gamma - \int_{L_s} \mathbf{u}^G \mathbf{NDB}_j d\Gamma \\ \qquad + \int_{L_s} \mathbf{p}^G \phi_j d\Gamma + \alpha_i \phi_j(\mathbf{x}_i) \text{ where } \mathbf{u}_i \text{ is unknown} \end{cases} \tag{29}$$

Here, $\mathbf{D}$ is the stress-strain matrix and

$$\mathbf{N} = \begin{bmatrix} n_1 & 0 & n_2 \\ 0 & n_2 & n_1 \end{bmatrix}; \quad \mathbf{B}_j = \begin{bmatrix} \phi_{j,1} & 0 \\ 0 & \phi_{j,2} \\ \phi_{j,2} & \phi_{j,1} \end{bmatrix} \tag{30}$$

The system presented in Eq.(26) can be solved by any conventional method, like Gauss elimination. Notice that

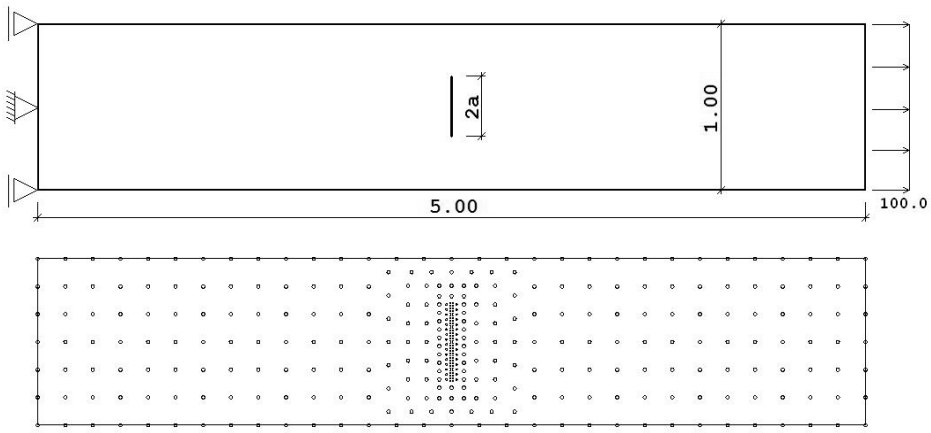

Figure 6 : Geometry and node cloud of examples 1 and 2

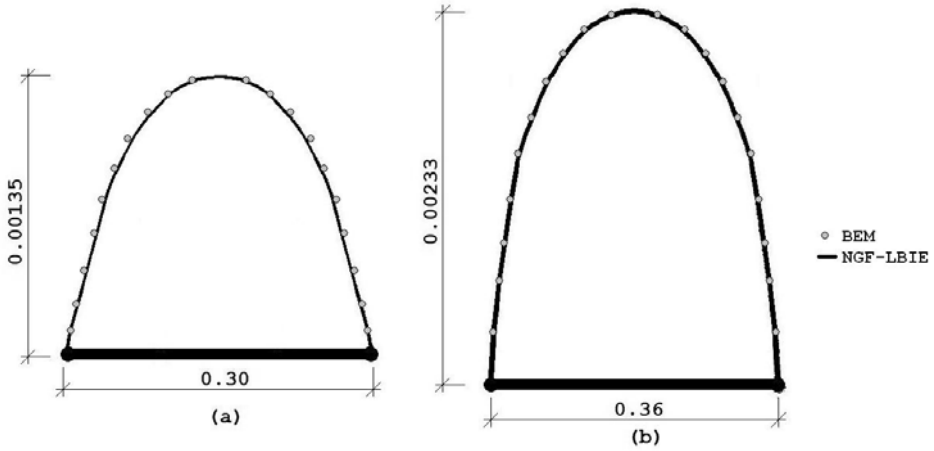

Figure 7 : Crack openings: (a) example 1; (b) example 2

the solution of the equations system is a vector containing the fictitious values $\hat{\mathbf{u}}_i$, which must be post-processed using Eq.(17) and its normal derivative in order to obtain the real values of displacements and tractions at all points.

The integrals involving $\mathbf{p}^G(\mathbf{x})$ in Γ_{su} have singularities of order $(1/r^2)$, which are computed using Kutt's quadrature [Telles, Castor and Guimarães (1995)]. Other schemes of integration applicable to the singular parts can also be found in [Sladek, Sladek, Atluri and van Keer (2000)], but due to its simplicity and accuracy, Kutt's method has been selected.

6 Examples

Three examples are presented in order to validate the NGF-LBIE procedure and they are all based on the same model (an axially loaded plate containing a crack). The difference between them is the actual results analyzed. In the first and second examples, the crack opening and the σ_{xx} stresses in the crack neighborhood are presented. In the last one, the stress intensity factor K_I is the result compared. For all examples presented, the relation (r_i/c_i) for the MLS weight function is equal to 4.0. This value can guarantee a good "decay" of w.

It can be seen that the adopted node cloud is denser in the neighborhood of the crack, but without any node positioned right on it. The distribution of nodes, influenced by the presence of the crack, can be uniform or not, but the crack tips must have denser clouds near them because of the natural difficulty in representing the behavior of stresses in that region. Good results were obtained when at least 10% of the total number of nodes is influenced by the crack. In addition, displacement discontinuity values

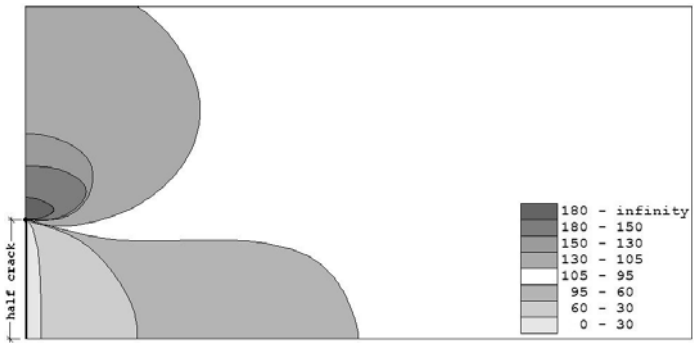

(a)

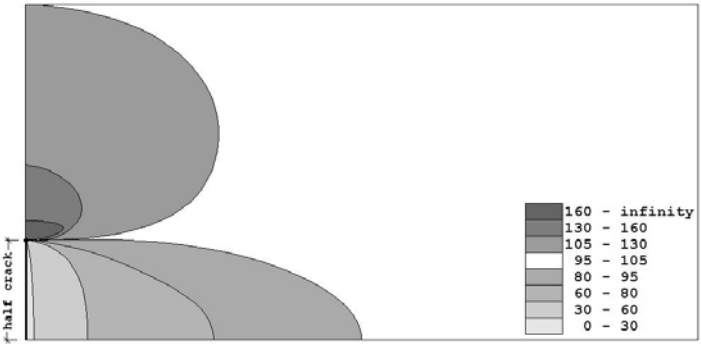

(b)

Figure 8 : σ_{xx} stress: (a) example 1; (b) example 2

have been computed over the crack surfaces by simple MLS extrapolations.

6.1 Crack opening and σ_{XX} stresses in the crack neighborhood

The first and second examples analyzed are presented in Fig.6 and the difference between them is only the value of $2a$, which for the first is 0.30 and for the second is 0.36. The nodes near the crack are equally distributed along its length. In both examples the Young modulus and Poisson's rate are $E = 10000$ and $\nu = 0.33$, and the number of nodes $N = 372$. The results are compared with a well-established BEM [Brebbia, Telles and Wrobel (1984)] code.

The results presented are the opening of the cracks (Fig.7) and the σ_{xx} stresses around the cracks (Fig.8, because of the symmetry, only the superior-right quadrant is shown). The results obtained by both methods were almost the same and the differences are imperceptible in Fig.8.

6.2 Stress intensity factor

Basically, this example is almost the same as the last two, varying a little bit in geometry, as depicted in Fig.9. Differently from the first example, the distribution of nodes near the crack is not uniform, but the node density close to the tips is still high. The results are compared with the ones presented in [Telles, Castor and Guimarães (1995)]. For this example it is considered: $E = 50000$, $\nu = 0.2$, number of nodes $N = 210$.

The stress intensity factor K_I is obtained here using the following relation [Barra and Telles (1999)]

$$K_I = \frac{G\sqrt{2\pi}}{4(1+\nu)} \sum_{i=1}^{np} \frac{c_{11}(\zeta_i,\zeta)\sqrt{r_i}}{r_i} \tag{31}$$

where G is the shear modulus, $c_{11}(\zeta_i,\zeta)$ is the value of the crack opening at node ζ_i, r_i is the distance between ζ_i and the nearest crack edge and $np=6$ is the number of nodes considered. The chosen positions of the nodes ζ_i are presented in Fig.10, in intrinsic coordinates.

The comparison of the results obtained with this technique and those found with NGF-BEM (numerical

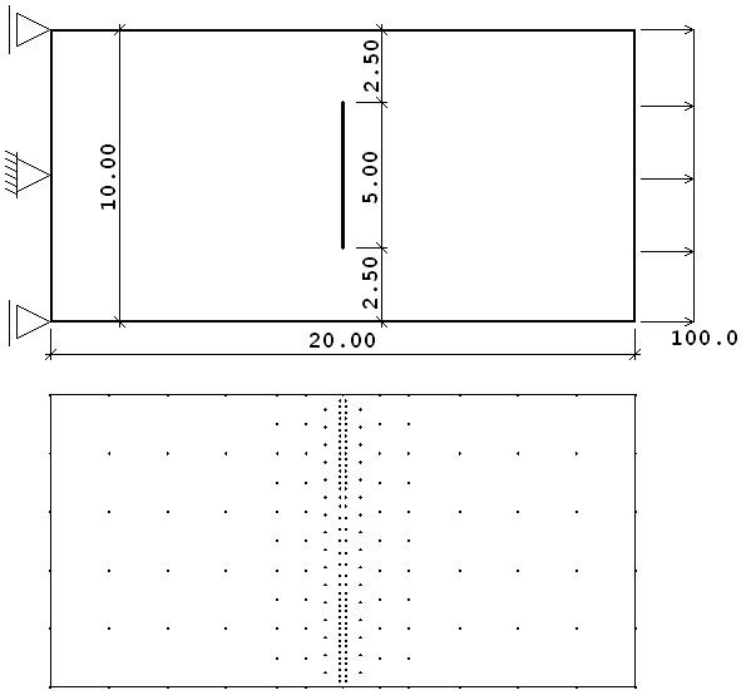

Figure 9 : geometry and node cloud of example 3

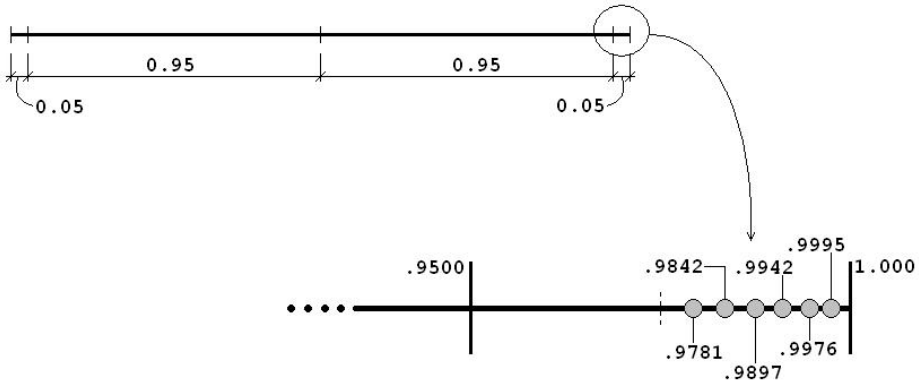

Figure 10 : Position of ζ_i for K_I calculation

Table 1 : Comparison of results

Method	K_I/K_0	Error (%)
NGF-LBIE	1.182	0.51
NGF-BEM	1.1877	0.99
AGF-BEM	1.1871	0.94
estimated	$1.176 \pm g\%$	-

Green's function with BEM) and AGF-BEM (analytical Green's function with BEM) are presented in Table 1

In order to present the results in non-dimensional form, they are divided by $K_0 = \sigma\sqrt{\pi a}$, where σ is the applied load and a is the half-length of the crack.

7 Conclusion

This work aimed at introducing the concept of the NGF for fracture mechanics into the context of the LBIE method. Here the LBIE formulation was presented for the elastostatic problem, as well as the procedure for obtaining the NGF for fracture mechanics and the MLS approximation scheme used to interpolate the trail function.

The results produced illustrate the accuracy of the NGF-

LBIE procedure and encourage new developments in this area of research.

References

Atluri, S. N.; Shen S. (2002): The meshless local Petrov-Galerkin (MLPG) method: a simple & less-costly alternative to the finite element and boundary element methods. *CMES: Computer Modeling in Engineering & Sciences,* vol. 3, n.1, pp. 11-51.

Atluri, S. N.; Sladek, J.; Sladek, V.; Zhu, T. (2000): The local boundary integral equation method (LBIE) and it's meshless implementation for linear elasticity. *Computational Mechanics*, vol. 25, pp. 180-198.

Gao, L.; Liu, K.; Liu Y. (2006): Applications of MLPG Method in Dynamic Fracture Problems. *CMES: Computer Modeling in Engineering & Sciences,* vol. 12, n.3, pp. 181-196.

Andreaus, U; Batra, R. C.; Porfiri, M. (2005): Vibrations of Cracked Euler-Bernoulli Beams using Meshless Local Petrov-Galerkin (MLPG) Method. *CMES: Computer Modeling in Engineering & Sciences,* vol. 9, n.2, pp. 111-132.

Sladek, J.; Sladek, V.; Krivacek, J.; Zhang, C. (2005): Meshless Local Petrov-Galerkin Method for Stress and Crack

Analysis in 3-D Axisymmetric FGM Bodies. *CMES: Computer Modeling in Engineering & Sciences,* vol. 8, n.3, pp. 259-270.

Telles, J. C. F.; Castor, G. S.; Guimarães, S. (1995): A numerical Green's function approach for boundary elements applied to fracture mechanics. *International Journal for Numerical Methods in Engineering*; vol. 38, pp. 3259-3274.

Miers, L. S.; Telles, J. C. F. (2005): Structural Integrity Analysis Using the Numerical Green's Function and the Local Boundary Integral Equation Method. *Structural Integrity & Durability*, vol. 1, n. 3, pp. 225-232.

Lancaster, P., Salkauskas, K. (1981): Surfaces generated by moving least squares methods. *Mathematics of Computations*, vol. 37, pp. 141-158.

Brebbia, C.A.; Telles, J. C.F.; Wrobel, L. C. (1984): Boundary Element Techniques: Theory and Application in Engineering. Springer: Berlin.

Chen, Y.; Eskandarian, A.; Oskard, M.; Lee, J. D. (2004): Meshless analysis of plasticity with application to crack growth problems. *Theoretical and Applied Fracture Mechanics*, vol. 41, pp. 83-94.

Sladek, V.; Sladek, J.; Atluri, S. N.; van Keer, R. (2000): Numerical integration of singularities in meshless implementation of local boundary integral equations. *Computational Mechanics*, vol. 25, pp. 394-403.

Barra, L. P. S.; Telles J. C. F. (1999): A Hypersingular Numerical Green's Function Generation for BEM Applied to Dynamic SIF Problems. *Engineering Analysis with Boundary Elements*, vol. 23, n. 1, pp. 77-87.

Vavourakis, V., Sellountos, E. J., Polyzos, D. (2006): A comparison study on different MLPG(LBIE) formulations. *CMES: Computer Modeling in Engineering & Sciences,* vol. 13, n.3, pp. 171-183.

Atluri, S. N., Zhu, T. (1998): A new Meshless Local Petrov-Galerkin (MLPG) approach in computational mechanics. *Computational Mechanics*, vol. 22, pp. 117-127.